sensors

MDPI

Article

Green Synthesis of Phosphorescent Carbon Dots for Anticounterfeiting and Information Encryption

Mingming Cheng [1], Lei Cao [1], Hanzhou Guo [2], Wenfei Dong [1,3] and Li Li [1,*]

[1] School of Biomedical Engineering (Suzhou), Division of Life Sciences and Medicine, University of Science and Technology of China, Hefei 230026, China; cmm13862591726@mail.ustc.edu.cn (M.C.); cl1221@mail.ustc.edu.cn (L.C.); wenfeidong@sibet.ac.cn (W.D.)
[2] Changchun Guoke Medical Engineer and Technology Development Co., Ltd., Changchun 130033, China; guohanzhou1@163.com
[3] CAS Key Laboratory of Biomedical Diagnostics, Suzhou Institute of Biomedical Engineering and Technology, Chinese Academy of Science (CAS), Suzhou 215163, China
* Correspondence: lil@sibet.ac.cn; Tel.: +86-15995709126

Abstract: Room-temperature phosphorescent (RTP) carbon dots (CDs) have promising applications in bioimaging, anticounterfeiting, and information encryption owing to their long lifetimes and wide Stokes shifts. Numerous researchers are interested in developing highly bright RTP CDs using environmentally friendly and safe synthesis processes (e.g., natural raw materials and zero-pollution production pathways). In this study, we successfully synthesized RTP CDs using a hydrothermal process employing natural vitamins as a raw material, ethylenediamine as a passivator, and boric acid as a phosphorescent enhancer, which is referred to as phosphorescent CD (PCD). The PCDs exhibit both bright blue fluorescence emission and green RTP emission, with a phosphorescence lifetime as long as 293 ms and an excellent green afterglow visible to the naked eye for up to 7.0 s. The total quantum yield is 12.69%. The phosphorescence quantum yield (PQY) is up to 5.15%. Based on the RTP performance, PCDs have been successfully employed for anticounterfeiting and information protection applications. The results of this study provide a green strategy for the scalable synthesis of RTP materials, which is a practical method for the fabrication of RTP materials with high efficiency and long afterglow lifetimes.

Keywords: room-temperature phosphorescent; carbon dots; anti-counterfeiting; information protection

Citation: Cheng, M.; Cao, L.; Guo, H.; Dong, W.; Li, L. Green Synthesis of Phosphorescent Carbon Dots for Anticounterfeiting and Information Encryption. *Sensors* **2022**, *22*, 2944. https://doi.org/10.3390/s22082944

Academic Editor: Giovanni Agati

Received: 4 March 2022
Accepted: 2 April 2022
Published: 12 April 2022

1. Introduction

Room-temperature phosphorescent (RTP) materials have attracted increasing attention because of their enormous potential in optoelectronics [1,2], ensing [3–5], imaging [6,7], and safe encryption [8–12]. Metal-doped inorganic [13,14] and organometallic compounds [15–17] are now the most effective RTP materials. However, these materials, which are frequently composed of rare metals, are expensive, cytotoxic, rigid, and unstable. Pure organic RTP materials [18–20], as an alternative, are less effective because of their low intersystem crossing (ISC) and rapid deactivation rate. Thus, it is very desirable to develop new metal-free RTP materials with low toxicity, environmental protection, long life, and low cost.

In recent years, novel zero-dimensional carbon nanomaterials, known as carbon dots (CDs), have attracted significant interest because of their low toxicity, biocompatibility, ease of manufacture, and remarkable optical properties [20,21]. However, generating phosphorescent CDs at room temperature is very challenging because of the instability of excited triplet species, oxygen-induced phosphorescence quenching, and inefficient intersystem crossover (ISC). There are two distinct strategies for achieving room-temperature phosphorescence in CDs. One method is to introduce heteroatoms, which facilitate efficient spin–orbit coupling and result in a low singlet–triplet splitting energy [22–24]. Typically,

nitrogen–phosphorus co-doped CDs are synthesized by microwave irradiation using triethanolamine as the carbon source and phosphoric acid as the dopant [25]. Another possibility is to embed CDs in various matrices, including polyvinyl alcohol [26,27], acrylamide [5,28], urea [1], trisodium citrate [2], aluminum sulfate [29], zeolite, silica [30–32], melamine [33,34], and boric acid (BA) [35,36]. Recently, by embedding CDs in a silica matrix, a 5.72-s long-life RTP material was developed. During this process, the adequate three-dimensional nano-space encompassed by the Si-O tetrahedra acts as a spatial constraint, substantially suppressing intramolecular vibrations, the development of stable covalent and hydrogen bonds between the rigid structure, and CDs successfully stabilizing their triplet excited states.

At present, many valuable methods for synthesizing phosphorescent CDs have been developed [37–39]. The main commonly used methods are one-step synthesis and two-step synthesis. The one-step method also includes the hydrothermal method, microwave method, heat treatment, etc. The reaction precursors such as different carbon sources, organic materials, heteroatoms, etc. are mixed, and then, the reaction temperature and time are selected to obtain the reaction products in one step. Although this method is simple and fast, the process of in situ growth of carbon dots on the substrate is highly uncontrollable and usually requires a strong driving force to achieve. Therefore, this approach is not generally considered [40–43]. However, the two-step approach is synthesizing carbon dots first and then embedding them into different substrates such as nanoporous materials, zeolites, polyvinyl alcohol, boric acid, etc. [40–46]. This method is more controllable and easier to implement than the one-step method [47]. Therefore, in this study, the two-step method was used to synthesize phosphorescent carbon dots [48].

It is well-known that the energy gap between the single and triplet states can be reduced by the boron atom, because B is an electron-absorbing atom. When BA is introduced into the CDs, it favors the ISC from S1 to T1, which enhances the phosphorescence emission of the triplet exciton [20,21]. In brief, when BA is used as a matrix, the generated glassy state prevents the CD's triplet excitons from being consumed nonradiative. Additionally, as an electron-attracting atom, boron possesses an empty p orbital that may attract transitions to create a p-conjugate system, thereby lowering the S1–T1 energy gap and increasing the rate of ISC [49–51]. More importantly, the covalent connections produced between the B and C atoms stabilize the overall system [36,37], thus facilitating RTP emission. Owing to these characteristics, BA is regarded as a promising matrix for the universal fabrication of CD-based RTP materials. However, very few studies have been conducted on the use of BA as a phosphorescent emission substrate.

Herein, by a two-step approach, we synthesize carbon dots first and then embed them into boric acid substrates (Figure 1). This method is more controllable and easier to implement than the one-step method [52]. Besides, we prepared phosphorescent CDs (PCDs) with vitamin B1, a natural vitamin, as the main raw material. The preparation process is nontoxic, harmless, and environment-friendly. The preparation RTP materials have low toxicity, environmental protection, and low costs. The prepared PCDs show excellent photoluminescence (PL) and phosphorescence. The total quantum yield is 12.69%. The phosphorescence quantum yield (PQY) is as high as 5.15%, the RTP life is 293 milliseconds, and the visible afterglow lasts more than 7 s. Owing to the excellent RTP performance, the PCDs have been successfully employed for anticounterfeiting and information protection applications.

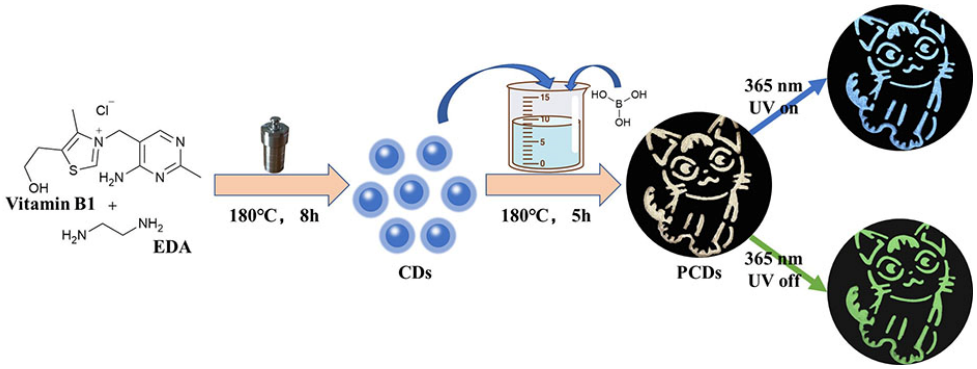

Figure 1. Schematic illustration of the synthesis process for the PCDs.

2. Materials and Methods

2.1. Chemicals and Materials

Thiamine hydrochloride (Vitamin B1), ethylenediamine (EDA), and boric acid (BA) were purchased from Titan Scientific (Shanghai, China). Ultrapure water was used throughout the whole experiment.

2.2. Instrumentation

High-resolution transmission electron microscopy (HR-TEM) pictures were collected at 100 kV using a TECNAI G2 microscope (Thermo Fisher, Waltham, MA, USA). The image of scanning electron micrographs (SEM) was measured by a XL-30ESEM FEG scanning electron microscope (FEI, Hillsboro, OR, USA). FTIR spectra were conducted with a VERTEX 70 FT-IR spectrometer (Bruker, Bremen, Germany). The X-ray photoelectron spectroscopy (XPS) spectra were acquired using an ESCALAB 250Xi spectrometer (Thermo Fisher, Waltham, MA, USA). A Rigaku Minister apparatus was used to generate the X-ray diffraction (XRD) patterns (Tokyo, Japan). The UV absorption spectra were performed via a Hitachi UV2450 spectrophotometer (Tokyo, Japan). The fluorescence spectra were obtained using an F97Pro FL spectrophotometer coupled with a 1.0-cm quartz cell (Lengguang Technology, Shanghai, China). Additionally, the fluorescent, phosphorescent lifetime, and emission spectrum were analyzed at room temperature using an FLS-1000 fluorescence spectrophotometer (Edinburgh, UK).

2.3. Synthesis of VB1-CDs

In general, 0.5 g of vitamin B1 was dissolved in 10 mL of ultrapure water initially, and then, 150 µL of EDA was dropped into the solution and ultrasonically dispersed well. Subsequently, the solution was transferred to a 20-mL poly(tetrafluoroethylene)-lined autoclave and reacted at 180 °C for 8 h in a drying oven. After the reaction, the centrifuge (8000 rpm, 10 min) removed the pellets and prepared them for usage.

2.4. Synthesis of PCDs

Basically, 50 µL, 100 µL, 500 µL, and 1000 µL of VB1-CD solutions were, respectively, added into small beakers, filled with 20-mL ultrapure water, and stirred evenly. Then, 3 g of boric acid was added into each beaker, covered with tin foil, and placed in a drying oven for reaction at 180 °C for 5 h. After the reaction, the materials were ground into powder; thus, PCD50, PCD100, PCD500, and PCD1000 were obtained, respectively.

2.5. Fabrication of LEDs

The central LED chips, which emit 395-nm UV and 460-nm blue light, were purchased from Shenzhen Prospect Technology Co (Shenzhen, China). The LEDs all operated at a voltage of 3.0 V. PCD100 powder was mixed with epoxy resin AB glue and then placed at the center of the LED chips. After drying in a 100 °C oven for one hour, LED beads were obtained.

3. Results and Discussion

3.1. Characterization and Optical Properties of VB1-CDs

Transmission electron microscopy (TEM) was performed to investigate the morphology of the VB1-CDs (Figure S11). The FTIR spectrum and XPS characterizations of VB1-CDs are shown in Figures S12 and S13. The measured XPS spectrum of VB1-CDs in Figure S13 clearly shows four peaks at 285.14, 400.16, 531.38, and 163.56 eV for C 1 s, N 1 s, O 1 s, and S 2 p, respectively. The elemental contents of the VB1-CDs were 73.96% C, 12.11% O, 11.84% N, and 2.46% S, respectively. A series of analyses such as FTIR and XPS on the VB1-CDs show that there are C=N and C=O in the materials, etc. C=N and C=O promote fluorescence emission. Steady-state spectroscopic investigations were conducted to elucidate the photophysical behavior of VB1-CDs. Figure 2 depicts the UV–Vis absorption, excitation, and fluorescence spectra of VB1-CDs. The UV absorption (Figure 2a) results in the formation of two humps at 271 and 320 nm, which are ascribed to the n–π* transition of C–O and C=O or C–N functional groups present at the margins of the VB1-CDs. The π→π* leap of the conjugated C=C unit in the carbon nucleus produces a strong absorption near 228 nm. The presence of these groups beneficially influences the fluorescence properties of the CDs [38,39]. The VB1-CDs exhibit an emission of 431 nm with excitation at 365 nm, with no noticeable absorption peak at 400 nm (Figure 2a). As shown in the inset of Figure 2b, the fluorescence wavelength is red-shifted from 423 to 525 nm, with a consistent increase in the excitation wavelength from 325 to 465 nm, demonstrating apparent excitation-dependent behavior. The highest excitation and emission wavelengths are 385 and 438 nm, respectively. The absolute quantum yield of VB1-CDs is 9.49%, and Figure 2c shows the fluorescence lifetime decay with a lifetime of 4.86 ns.

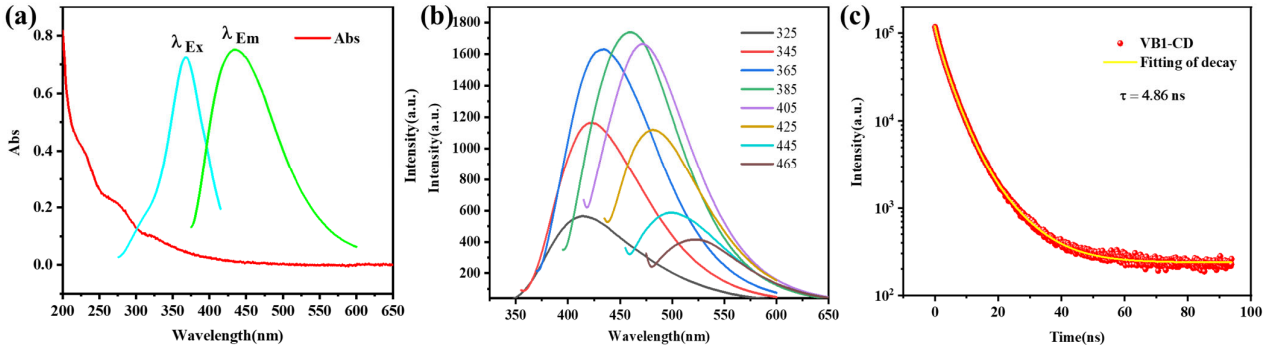

Figure 2. (**a**) UV–Vis absorption of VB1-CDs. (**b**) PL emission spectra of VB1-CDs aqueous solution. (**c**) Fluorescence lifetime decay of VB1-CDs.

3.2. Characterization of PCDs

Taking PCD100 as an example, transmission electron microscopy (TEM) was performed to investigate the morphology and particle distributions of the PCDs, which demonstrates that the PCDs are evenly distributed as spherical shapes with an average size of 2.3 nm (Figure 3a). The size distribution of PCD100 is shown in Figure S9, and the results indicate that the diameters of PCD100 range from 1.03~3.98 nm. Additionally, PCD100 has a lattice fringe spacing of 0.21 nm, which is consistent with the categorization of graphite carbon. Figure S10 shows the scanning electron microscope (SEM) images of the powders of PCD100 [25,40].

To further investigate the functional groups and chemical composition of the PCDs, Fourier-transform infrared spectroscopy (FTIR) and X-ray photoelectron spectroscopy (XPS) techniques were applied. PCD100 exhibits a wide FTIR absorption band between 2500 and 3500 cm^{-1}, as depicted in Figure 3b, indicating the presence of O-H (3250 cm^{-1}) on the exterior. In addition, the peaks at 1484 cm^{-1} are ascribed to the stretching vibrations of C–N. Stretching vibrations of hydrogen-bonded C–O–B (1232 cm^{-1}) and C–B (911 cm^{-1}) are observed, demonstrating the presence of B doping in the PCDs [35].

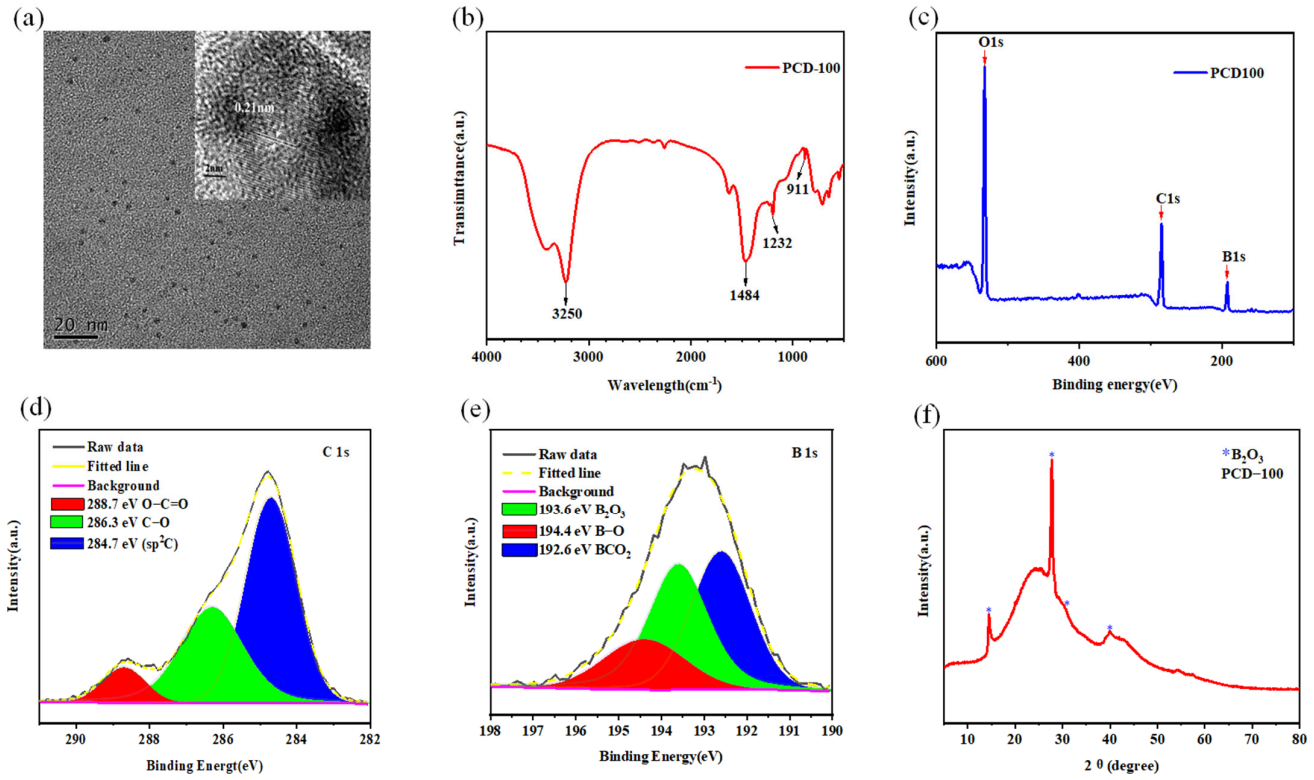

Figure 3. (**a**) TEM image of PCD100. (**b**) FTIR spectrum of PCD100. (**c**) Full-scan XPS spectrum of PCD100. (**d**) HR XPS C1s. (**e**) HR XPS B1s. (**f**) XRD pattern of PCD100.

The presence of O, C, and B are visible in the full-scan XPS spectrum of PCD100 (Figure 3c), with atomic percentages of 38.3%, 32.18%, and 27.45%, respectively. The characteristic peaks for O1, C1, and B1s are 531.08 eV, 285.08 eV, and 193.08 eV, respectively. The XPS spectra of C1s at high resolution (HR) display three components: C–C/C=C (284.7 eV), C–O (286.3 eV), and C=O=O (288.7 eV) (Figure 3d). The three peaks in the HR B1s XPS spectra at 192.6 eV, 193.6 eV, and 194.4 eV are assigned to BCO2, B2O3, and B-O, respectively (Figure 3e) [41–43]. The XPS results are compatible with the FTIR findings. X-ray diffraction (XRD) analysis of PCD100 shows characteristic B2O3 peaks at 14.5°, 27.4°, 30.2°, and 40.0° (Figure 3f).

3.3. Optical Properties of PCDs

The photophysical characteristics of PCD100 were investigated thoroughly. The UV–Vis absorption spectra of the PCD100 aqueous solution exhibit three peaks at 220, 260, and 322 nm (Figure 4a). The first one is assigned to the π–π* transformation of C=C, while the last two emerge from the n–π* transformation of C=O [41]. The PL spectra of the PCD100 aqueous solution exhibit excitation-dependent characteristics, with the greatest emission occurring at 430 nm under 365-nm excitation (Figure 4b). However, no afterglow is observed in the PCD100 solution, which is attributed to molecular rotation, vibration, and collisional triplet relaxation. The emission of solid PCD100 fluorescence (Figure 4c) and phosphorescence (Figure 4d) are excitation-dependent, with the highest emissions at 496 nm and 570 nm, respectively. The fluorescence emission of solid PCD100 moves gradually from 431 to 507 nm as the excitation wavelength increases (Figure 4c).

The maximum PQY of PCD100 is as high as 5.15%, which is why PCD100 produces bright blue light when exposed to a UV lamp (254 nm) and still leaves a light-green afterglow visible to the naked eye when the lamp is turned off, which lasts for about 3 s (Figure 5a). Furthermore, when excited at 365 nm, PCD100 emits blue fluorescence, and ultralong-lived yellow-green RTP is identified up to 7 s after the excitation source is removed (Figure 5b). As shown in Figure 5c, the degradation of PCD100 can be modeled

using a triexponential function, and the average lifetime is determined to be 293 ms at 365-nm excitation. The fluorescence lifetime decay is shown in Figure 5d, and the lifetime is 5.50 ns. These findings suggest that the presence of several triple-excited states may be responsible for the excitation-dependent properties of PCD100. The elimination of the afterglow in the solution implies that the performance of RTP may be stabilized in the solid state. In order to understand our research results more clearly, we compared them with previous studies in terms of RTP lifetime and PQY, and the results are shown in Table S6.

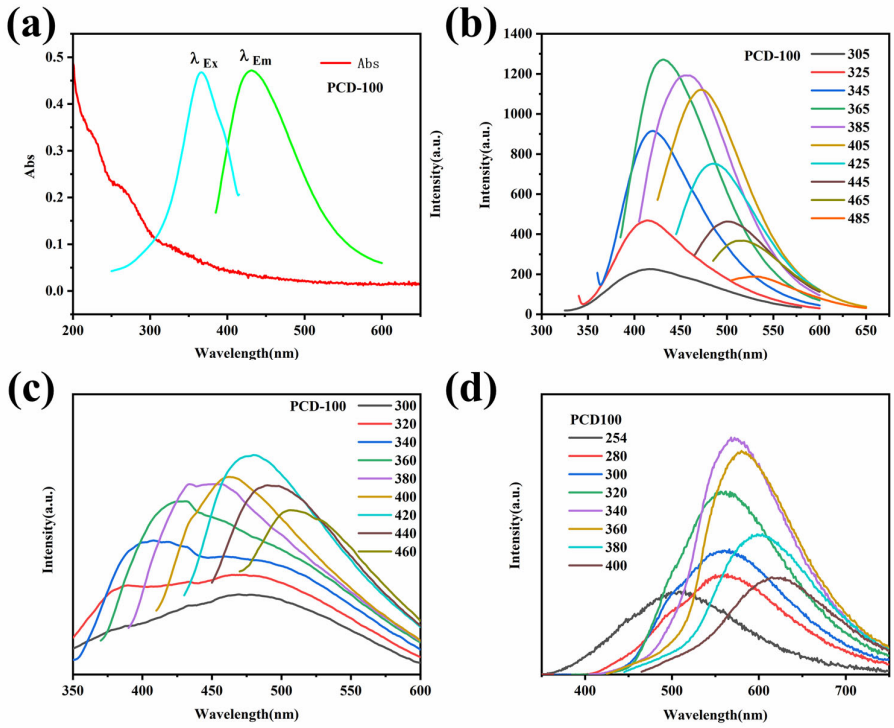

Figure 4. (**a**) UV–Vis absorption and PL excitation and emission spectra of PCD100 aqueous solution. (**b**) PL emission spectra of PCD100 aqueous solution. (**c**) PL emission spectra of PCD100 solid. (**d**) Phosphorescence emission spectra of PCD100 solid.

To elucidate the nature of the RTP, a series of controlled studies were conducted. No RTP is identified when only VB1-CD or BA is used as a precursor. Under identical conditions, 3 g of BA interacted with various masses (50, 500, and 1000 μL) of VB1-CD to produce the PCDs, named PCD-50, PCD-500, and PCD-1000, respectively. PCD-50, PCD-500, and PCD-1000 have absorption spectra identical to those of BD50, exhibiting three characteristic peaks at 224, 252, and 323 nm (Figure S1). The PL spectra of PCD-50 (Figure S2a), PCD-500 (Figure S2b), and PCD-1000 (Figure S2c) aqueous solution exhibited excitation-dependent characteristics, with the greatest emission occurring at 432, 474, and 473 nm under 365, 405, and 405-nm excitation, respectively. PCD-50, PCD-500, and PCD-1000 solids display excitation-dependent PL characteristics, with emission peaks at 474, 488, and 500 nm, respectively, when excited at 420 nm (Figure S2d–f, respectively). Figure S3 shows the phosphorescence spectra of PCD-50, PCD-500, and PCD-1000, with the greatest emission occurring at 521, 539, and 551 nm under 340, 380, and 380-nm excitation, respectively. The average fluorescence lifetime of PCD-50, PCD-500, and PCD-1000 is 5.33, 5.51, and 5.41 ns, respectively (Figure S4a–c; Table S1). When activated by a UV lamp at 254 nm, PCD50 emits light-blue light, PCD500 emits light-yellow light, and PCD1000 emits orange light (Video S1). When the UV light at 254 nm is shut off, PCD50 displays a very weak green RTP that lasts 3 s, whereas PCD500 displays a very weak pale yellow RTP that lasts only 2 s. However, when the 365-nm UV light is shut off, PCD50 displays a strong green RTP that is visible to the human eye for 6 s, PCD500 displays a green RTP that is visible to the naked eye for 5 s, and PCD1000 displays a light-green RTP for 3 s

(Figure S5a–c and Video S2). The total quantum yield of PCD-50, PCD-500, and PCD-1000 are 12.08%, 7.18%, and 4.65%, respectively. By calculating the spectral integrated area, the PQYs of PCD-50, PCD-500, and PCD-1000 are 4.25%, 4.00%, and 2.82%, respectively [53,54]. The average lifetime (Figure S4d–f and Table S2) of PCD-50, PCD-500, and PCD-1000 reduces from 292, 207, and 152 ms, respectively. Based on the findings mentioned above, the fluorescence and phosphorescence properties of PCD100 are the best.

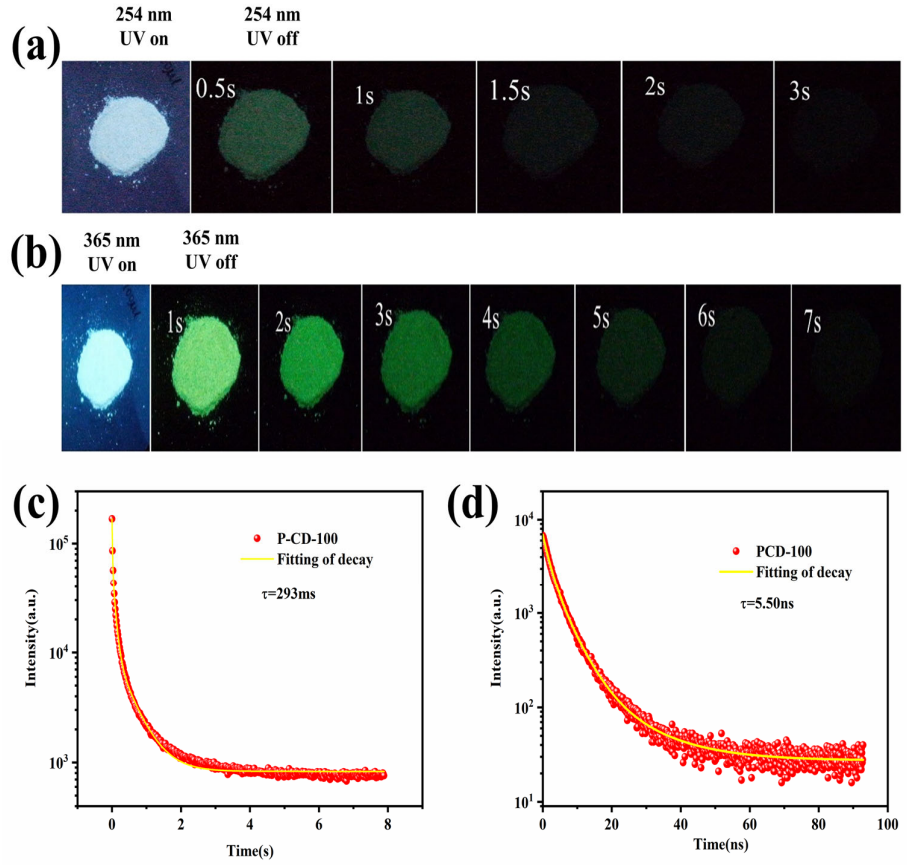

Figure 5. (**a**) Photographs of PCD100 with a 254-nm UV lamp on and off. (**b**) Photographs of PCD100 with a 365-nm UV lamp on and off. (**c**) RTP lifetime decay of PCD100 solid under the excitation of 365 nm. (**d**) Fluorescence lifetime decay of PCD100 solution.

The XRD patterns of PCD-50, PCD-500, and PCD-1000 exhibit distinctive peaks comparable to those of PCD-100 (Figure S6). XPS analysis was used to identify the chemical compositions of PCD-50, PCD-500, and PCD-1000 (Figure S7). The B contents of PCD-50, PCD-500, and PCD-1000 are 32.93%, 34.52%, and 27.35%, respectively (Table S3). The S contents of PCD-50, PCD-500, and PCD-1000 are 0.81%, 1.51%, and 0.52%, respectively (Table S5). These findings suggest that the B–C covalent connections produced between VB1-CDs and BA may enhance the RTP characteristics of the PCDs. The FTIR spectra of PCD-50, PCD-500, and PCD-1000, which are comparable to those of PCD100, are shown in Figure S8.

Taking PCD50 and PCD100 as examples, we measured their fluorescence and phosphorescence spectral data on day 1 and day 7, respectively, and compared the data to verify the stability of the material (Figure S14). The results show that the spectral values of PCDs are slightly decreased, but the changes are not very large, so we can assume that the fluorescence and phosphorescence properties of phosphorescent carbon dots are more stable.

Considering the prior discussion, we propose a plausible mechanism for the phosphorescence of the PCDs. First, the C=O=O bonds in PCDs can induce RTP. Second, BA is necessary for synthesizing RTP, which may generate C–B bonds when combined with

VB1-CD. The covalent bonds and nanoconfined space of BA may prevent the extinguishing of excited triplet excitons, resulting in the facilitation of RTP emission. Based on the PL spectrum and the phosphorescence emission spectrum of PCD50 and PCD100. According to this formula, EST = h/k × C/λ = 1240/λ, the energy gaps (ΔE_{ST}) between the lowest single (S1) and triplet (T1) states were calculated to be equal to 0.42 eV and 0.43 eV, which are small values, allowing an effective ISC process to occur (Table S4) [35,36,54].

3.4. Application in LED, Anticounterfeiting, and Information Security

The high-efficiency blue-green fluorescence–phosphorescence emission of PCDs, together with their low cost and environmental friendliness, make them attractive candidates for use in high-performance single-component white light-emitting diodes (WLEDs). The LED chips operate at a voltage of 3 V and a current of 150 mA. The UV-pumped WLED was fabricated by mixing PCD100 powder with epoxy resin AB glue and then placed at the center of the 395-nm UV-LED chips and 460-nm blue LED chips. At a voltage of 3.0 V, the 395-nm UV LED produces efficient white emission. In addition, the LED exhibits green phosphorescence when the voltage is withdrawn (Video S3). As shown in Figure 6b, highly efficient single-component WLEDs based on PCDs have electroluminescence (EL) spectrum in the range 380~750 nm. Two separate peaks are visible at 450 nm for blue fluorescence and 570 nm for green phosphorescence emission. The 395-nm UV LED generates white light with CIE color coordinates of (0.26, 0.30). The coordinates of the 460-nm blue LED are (0.17, 0.16) (Figure 6a), and the emission spectrum of the as-fabricated LEDs is shown in Figure 6b [42,43].

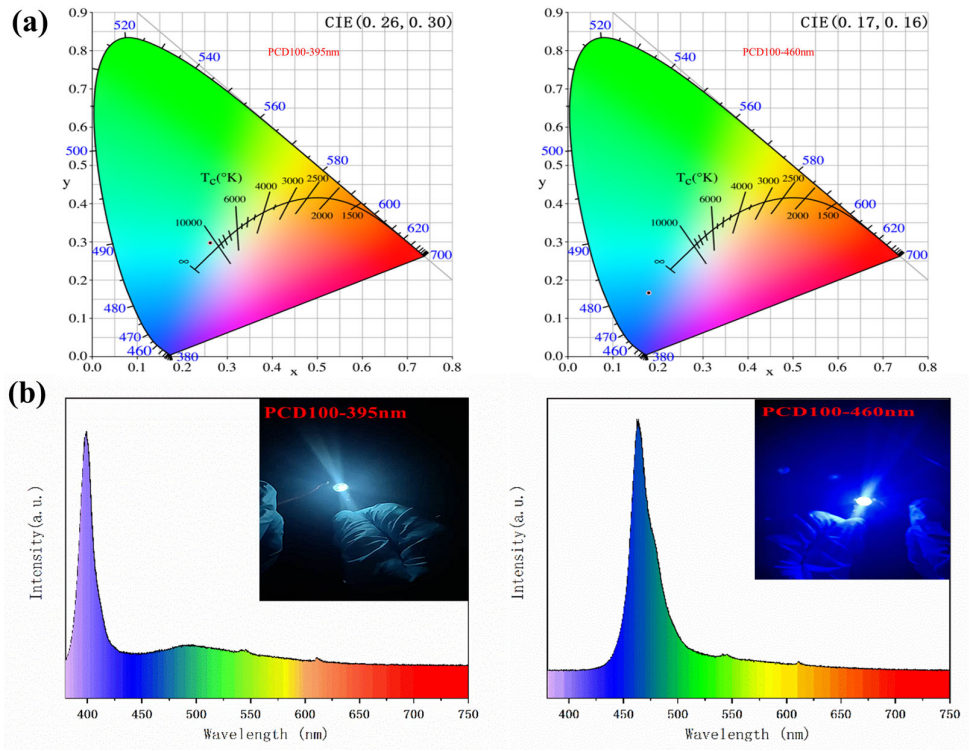

Figure 6. (**a**) CIE color coordinate of the WLED. (**b**) Emission spectrum of the WLED with UV.

In addition, PCDs have significant potential in the anticounterfeiting and information security domains because of their higher URTP capacity. First, PCD100 was utilized as a model to illustrate its potential application as a smart material for security protection. Figure 7a displays a typical triple-modal switching encryption created by placing PCD100 powder into the molds. In daylight, the theme is white. When exposed to 365-nm light, the pattern fluoresces blue. A brilliant green RTP pattern emerges when the light is switched off. Furthermore, Figure 7b demonstrates the use of PCD powders for information encryption.

The letters U and T, constructed of PCD100, are visible and display blue PL when excited at 365 nm. However, the letters S and C, made of non-phosphorescent material, produce yellow fluorescence. After deactivating the excitation, the green RTP emission "U T" could be distinguished from "USTC."

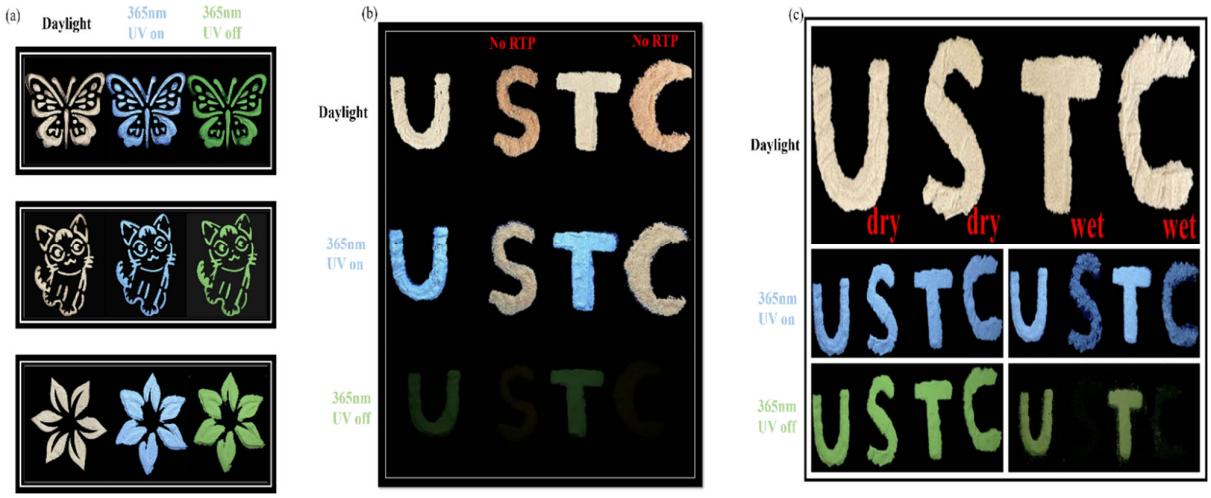

Figure 7. (**a**) Triple modal switching application of PCD100. (**b**) Anticounterfeiting application of PCD100. (**c**) Data encryption application of dry and wet PCD100.

Moreover, PCD100 can also be employed for anticounterfeiting purposes, because its phosphorescent emission is quenched by water. As shown in Figure 7c, the letters USTC are spelled out using PCD100; water is sprayed onto the second letter S and the fourth letter C. During the day, these four letters are hardly distinguishable. The initial letter U and the third letter T emit a blue glow when irradiated with 365-nm light. In comparison, the second letter S and the fourth letter C emit faint blue fluorescence. Only the first letter U and third letter T can be recognized as bright green phosphorescence when the UV lamp is switched off. These results indicate the practical use of PCDs in sophisticated anticounterfeiting and information protection applications.

4. Conclusions

We present a simple, environmentally friendly, and cost-effective method for generating RTP PCDs. PCD100 materials exhibit a high PQY (5.15%) value when excited at 365 nm. In addition, PCD100 has a long RTP lifetime of 293 ms with a visible afterglow duration of 7 s. Furthermore, PCDs have been effectively implemented for anticounterfeiting and data encryption. This study demonstrated a straightforward and highly successful approach for the synthesis of novel RTP luminophores utilizing commonly available and economic materials.

Supplementary Materials: The following supporting information can be downloaded at https://www.mdpi.com/article/10.3390/s22082944/s1.

Author Contributions: Conceptualization, W.D. and L.L.; Data curation, M.C.; Formal analysis, M.C.; Funding acquisition, W.D.; Methodology, L.C. and H.G.; Software, L.C. and H.G.; Writing—original draft, M.C. and L.L.; and Writing—review and editing, L.L. All authors have read and agreed to the published version of the manuscript.

Funding: This research was funded by the National Key R&D Program of China (Grand No. 2020YFC2004600); the National Natural Science Foundation of China (Grand No. 21803075, 91959112, 81902166, 62027825, and 82172077); the Science Foundation of the Chinese Academy of Sciences (No. 2020SYHZ0041); the Instrument Developing Project of Chinese Academy of Science (YJKYYQ20200038); the Primary Research & Development Plan of Jiangsu Province (BE2019683); and the Science and Technology Department of Jinan City (2018GXRC016).

Institutional Review Board Statement: Not applicable.

Informed Consent Statement: Not applicable.

Data Availability Statement: Not applicable.

Conflicts of Interest: The authors declare no conflict of interest.

References

1. Li, Q.; Zhou, M.; Yang, Q.; Wu, Q.; Shi, J.; Gong, A.; Yang, M. Efficient Room-Temperature Phosphorescence from Nitrogen-Doped Carbon Dots in Composite Matrices. *Chem. Mater.* **2016**, *28*, 8221–8227. [CrossRef]
2. Shen, C.-L.; Zang, J.-H.; Lou, Q.; Su, L.-X.; Li, Z.; Liu, Z.-Y.; Dong, L.; Shan, C.-X. In-situ embedding of carbon dots in a trisodium citrate crystal matrix for tunable solid-state fluorescence. *Carbon* **2018**, *136*, 359–368. [CrossRef]
3. Fu, M.; Feng, Z.; Wang, J.; Zhu, Y.; Gan, L.; Yang, X. Creatine-based carbon dots with room-temperature phosphorescence employed for the dual-channel detection of warfarin. *Appl. Surf. Sci.* **2022**, *571*, 151298. [CrossRef]
4. Gui, R.; He, W.; Jin, H.; Sun, J.; Wang, Y. DNA assembly of carbon dots and 5-fluorouracil used for room-temperature phosphorescence turn-on sensing of AFP and AFP-triggered simultaneous release of dual-drug. *Sens. Actuators B* **2018**, *255*, 1623–1630. [CrossRef]
5. Nie, Y.; Lai, W.; Zheng, N.; Weng, W. Multifunctional room-temperature phosphorescent carbon dots for relative humidity determination and information encryption. *Talanta* **2021**, *233*, 122541. [CrossRef]
6. Feng, Q.; Xie, Z.; Zheng, M. Room temperature phosphorescent carbon dots for latent fingerprints detection and in vivo phosphorescence bioimaging. *Sens. Actuators B* **2022**, *351*, 130976. [CrossRef]
7. Liang, Y.-C.; Gou, S.-S.; Liu, K.-K.; Wu, W.-J.; Guo, C.-Z.; Lu, S.-Y.; Zang, J.-H.; Wu, X.-Y.; Lou, Q.; Dong, L.; et al. Ultralong and efficient phosphorescence from silica confined carbon nanodots in aqueous solution. *Nano Today* **2020**, *34*, 100900. [CrossRef]
8. Gao, Y.; Zhang, H.; Shuang, S.; Dong, C. Visible—Light—Excited Ultralong—Lifetime Room Temperature Phosphorescence Based on Nitrogen-Doped Carbon Dots for Double Anticounterfeiting. *Adv. Opt. Mater.* **2020**, *8*, 1901557. [CrossRef]
9. Jiang, K.; Gao, X.; Feng, X.; Wang, Y.; Li, Z.; Lin, H. Carbon Dots with Dual-Emissive, Robust, and Aggregation-Induced Room-Temperature Phosphorescence Characteristics. *Angew. Chem. Int. Ed. Engl.* **2020**, *59*, 1263–1269. [CrossRef]
10. Jiang, K.; Wang, Y.; Cai, C.; Lin, H. Conversion of Carbon Dots from Fluorescence to Ultralong Room-Temperature Phosphorescence by Heating for Security Applications. *Adv. Mater.* **2018**, *30*, e1800783. [CrossRef]
11. Jiang, K.; Wang, Y.; Gao, X.; Cai, C.; Lin, H. Facile, Quick, and Gram-Scale Synthesis of Ultralong-Lifetime Room-Temperature-Phosphorescent Carbon Dots by Microwave Irradiation. *Angew. Chem. Int. Ed. Engl.* **2018**, *57*, 6216–6220. [CrossRef]
12. Long, P.; Feng, Y.; Cao, C.; Li, Y.; Han, J.; Li, S.; Peng, C.; Li, Z.; Feng, W. Self-Protective Room-Temperature Phosphorescence of Fluorine and Nitrogen Codoped Carbon Dots. *Adv. Funct. Mater.* **2018**, *28*, 1800791. [CrossRef]
13. Pacheco, M.E.; Castells, C.B.; Bruzzone, L. Mn-doped ZnS phosphorescent quantum dots: Coumarins optical sensors. *Sens. Actuators B* **2017**, *238*, 660–666. [CrossRef]
14. Shi, W.; Yao, J.; Bai, L.; Lu, C. Defect-Stabilized Triplet State Excitons: Toward Ultralong Organic Room-Temperature Phosphorescence. *Adv. Funct. Mater.* **2018**, *28*, 1804961. [CrossRef]
15. Dong, X.; Wei, L.; Su, Y.; Li, Z.; Geng, H.; Yang, C.; Zhang, Y. Efficient long lifetime room temperature phosphorescence of carbon dots in a potash alum matrix. *J. Mater. Chem.* **2015**, *3*, 2798–2801. [CrossRef]
16. Song, Z.; Liu, Y.; Lin, X.; Zhou, Z.; Zhang, X.; Zhuang, J.; Lei, B.; Hu, C. Multiemissive Room-Temperature Phosphorescent Carbon Dots@ZnAl2O4 Composites by Inorganic Defect Triplet-State Energy Transfer. *ACS Appl. Mater. Interfaces* **2021**, *13*, 34705–34713. [CrossRef]
17. Xiong, F.B.; Lin, H.F.; Meng, X.G.; Shen, H.X.; Zhu, W.Z. Photoluminescence properties of a novel red-emitting Pr3+-doped borate phosphor. *Optik* **2018**, *159*, 102–107. [CrossRef]
18. Chai, Z.; Wang, C.; Wang, J.; Liu, F.; Xie, Y.; Zhang, Y.Z.; Li, J.R.; Li, Q.; Li, Z. Abnormal room temperature phosphorescence of purely organic boron-containing compounds: The relationship between the emissive behaviorand the molecular packing, and the potential related applications. *Chem. Sci.* **2017**, *8*, 8336–8344. [CrossRef]
19. Li, M.; Cai, X.; Qiao, Z.; Liu, K.; Xie, W.; Wang, L.; Zheng, N.; Su, S.J. Achieving high-efficiency purely organic room-temperature phosphorescence materials by boronic ester substitution of phenoxathiine. *Chem. Commun.* **2019**, *55*, 7215–7218. [CrossRef]
20. Wei, X.; Yang, J.; Hu, L.; Cao, Y.; Lai, J.; Cao, F.; Gu, J.; Cao, X. Recent advances in room temperature phosphorescent carbon dots: Preparation, mechanism, and applications. *J. Mater. Chem.* **2021**, *9*, 4425–4443. [CrossRef]
21. Jia, J.; Lu, W.; Gao, Y.; Li, L.; Dong, C.; Shuang, S. Recent advances in synthesis and applications of room temperature phosphorescence carbon dots. *Talanta* **2021**, *231*, 122350. [CrossRef]
22. Gao, Y.; Han, H.; Lu, W.; Jiao, Y.; Liu, Y.; Gong, X.; Xian, M.; Shuang, S.; Dong, C. Matrix-Free and Highly Efficient Room-Temperature Phosphorescence of Nitrogen-Doped Carbon Dots. *Langmuir* **2018**, *34*, 12845–12852. [CrossRef]
23. Liu, P.; Liu, C.; Chen, J.; Wang, B. Facile Synthesis of Matrix-Free Room-Temperature Phosphorescent Nitrogen-Doped Carbon Dots and Their Application as Security Inks. *Macromol. Mater. Eng.* **2021**, *306*, 2100339. [CrossRef]

24. Wang, Z.; Shen, J.; Sun, J.; Xu, B.; Gao, Z.; Wang, X.; Yan, L.; Zhu, C.; Meng, X. Ultralong-lived room temperature phosphorescence from N and P codoped self-protective carbonized polymer dots for confidential information encryption and decryption. *J. Mater. Chem.* **2021**, *9*, 4847–4853. [CrossRef]
25. Su, Q.; Lu, C.; Yang, X. Efficient room temperature phosphorescence carbon dots: Information encryption and dual-channel pH sensing. *Carbon* **2019**, *152*, 609–615. [CrossRef]
26. Chen, Y.; He, J.; Hu, C.; Zhang, H.; Lei, B.; Liu, Y. Room temperature phosphorescence from moisture-resistant and oxygen-barred carbon dot aggregates. *J. Mater. Chem.* **2017**, *5*, 6243–6250. [CrossRef]
27. Huang, J.; Zhu, J.; Yang, G.; Zhu, Y.; Xu, X.; Pan, G. Lifetime-tunable green room temperature phosphorescence of carbon dots by the multi-step modification. *Opt. Express* **2021**, *29*, 41014–41022. [CrossRef]
28. Li, H.; Ye, S.; Guo, J.-q.; Kong, J.-t.; Song, J.; Kang, Z.-h.; Qu, J.-l. The design of room-temperature-phosphorescent carbon dots and their application as a security ink. *J. Mater. Chem.* **2019**, *7*, 10605–10612. [CrossRef]
29. Joseph, J.; Anappara, A.A. Long Life-time Room-temperature Phosphorescence of Carbon Dots in Aluminum Sulfate. *ChemistrySelect* **2017**, *2*, 4058–4062. [CrossRef]
30. Sun, Y.; Liu, J.; Pang, X.; Zhang, X.; Zhuang, J.; Zhang, H.; Hu, C.; Zheng, M.; Lei, B.; Liu, Y. Temperature-responsive conversion of thermally activated delayed fluorescence and room-temperature phosphorescence of carbon dots in silica. *J. Mater. Chem.* **2020**, *8*, 5744–5751. [CrossRef]
31. Sun, Y.; Liu, S.; Sun, L.; Wu, S.; Hu, G.; Pang, X.; Smith, A.T.; Hu, C.; Zeng, S.; Wang, W.; et al. Ultralong lifetime and efficient room temperature phosphorescent carbon dots through multi-confinement structure design. *Nat. Commun.* **2020**, *11*, 5591. [CrossRef]
32. Jiang, K.; Wang, Y.; Cai, C.; Lin, H. Activating Room Temperature Long Afterglow of Carbon Dots via Covalent Fixation. *Chem. Mater.* **2017**, *29*, 4866–4873. [CrossRef]
33. Gao, Y.; Zhang, H.; Jiao, Y.; Lu, W.; Liu, Y.; Han, H.; Gong, X.; Shuang, S.; Dong, C. Strategy for Activating Room-Temperature Phosphorescence of Carbon Dots in Aqueous Environments. *Chem. Mater.* **2019**, *31*, 7979–7986. [CrossRef]
34. Li, Q.; Zhou, M.; Yang, M.; Yang, Q.; Zhang, Z.; Shi, J. Induction of long-lived room temperature phosphorescence of carbon dots by water in hydrogen-bonded matrices. *Nat. Commun.* **2018**, *9*, 734. [CrossRef]
35. Feng, Q.; Xie, Z.; Zheng, M. Colour-tunable ultralong-lifetime room temperature phosphorescence with external heavy-atom effect in boron-doped carbon dots. *Chem. Eng. J.* **2021**, *420*, 127647. [CrossRef]
36. Li, W.; Zhou, W.; Zhou, Z.; Zhang, H.; Zhang, X.; Zhuang, J.; Liu, Y.; Lei, B.; Hu, C. A Universal Strategy for Activating the Multicolor Room-Temperature Afterglow of Carbon Dots in a Boric Acid Matrix. *Angew. Chem. Int. Ed. Engl.* **2019**, *58*, 7278–7283. [CrossRef]
37. Jiang, W.; Liu, L.; Wu, Y.; Zhang, P.; Li, F.; Liu, J.; Zhao, J.; Huo, F.; Zhao, Q.; Huang, W. A green-synthesized phosphorescent carbon dot composite for multilevel anti-counterfeiting. *Nanoscale Adv.* **2021**, *3*, 4536–4540. [CrossRef]
38. Lin, L.; Zhou, S.; Guo, H.; Chen, Y.; Lin, S.; Yan, L.; Li, K.; Li, J. Nitrogen-doped carbon dots as an effective fluorescence enhancing system for the determination of perfluorooctyl sulfonate. *Mikrochim. Acta.* **2019**, *186*, 380. [CrossRef]
39. Wu, F.; Yang, M.; Zhang, H.; Zhu, S.; Zhu, X.; Wang, K. Facile synthesis of sulfur-doped carbon quantum dots from vitamin B1 for highly selective detection of Fe3+ ion. *Opt. Mater.* **2018**, *77*, 258–263. [CrossRef]
40. Zhou, Z.; Song, Z.; Liu, J.; Lei, B.; Zhuang, J.; Zhang, X.; Liu, Y.; Hu, C. Energy Transfer Mediated Enhancement of Room-Temperature Phosphorescence of Carbon Dots Embedded in Matrixes. *Adv. Opt. Mater.* **2021**, *10*, 2100704. [CrossRef]
41. Han, S.; Lian, G.; Zeng, X.; Cao, Z.; Wang, Q.; Cui, D.; Wong, C.-P. Water-soluble boron carbon oxynitride dots with excellent solid-state fluorescence and ultralong room-temperature phosphorescence. *Nano Res.* **2020**, *13*, 3261–3267. [CrossRef]
42. Wang, Z.; Liu, Y.; Zhen, S.; Li, X.; Zhang, W.; Sun, X.; Xu, B.; Wang, X.; Gao, Z.; Meng, X. Gram-Scale Synthesis of 41% Efficient Single-Component White-Light-Emissive Carbonized Polymer Dots with Hybrid Fluorescence/Phosphorescence for White Light-Emitting Diodes. *Adv. Sci.* **2020**, *7*, 1902688. [CrossRef]
43. Yuan, T.; Yuan, F.; Li, X.; Li, Y.; Fan, L.; Yang, S. Fluorescence-phosphorescence dual emissive carbon nitride quantum dots show 25% white emission efficiency enabling single-component WLEDs. *Chem. Sci.* **2019**, *10*, 9801–9806. [CrossRef]
44. Ru, L.; Lijun, H.; Ao, Y.; Jinjing, W.; Chunman, J.; Jianwei, L. A micro-wave strategy for synthesizing room temperature phosphorescent materials. *Chin. Chem. Lett.* **2022**, *33*, 1001–8417.
45. Shuai, W.; Jing, W.; Qiu, H.; Xin, Z.; Zi, Y.; Sheng, X.; Qi, L.; Zheng, L. Greatness in Simplicity: Efficient Red Room-Temperature Phosphorescence from Simple Halogenated Maleimides with a 2D Layered Structure. *ACS Appl. Mater. Interfaces* **2022**, *14*, 14703–14711. [CrossRef]
46. Fen, M.; Wei, X.; Bin, L.; Zhen, Z.; Yan, F.; Hui, C.; Qing, H.; Jian, C. In Situ Turn-On Room Temperature Phosphorescence and Vapor Ultra-sensitivity at Lifetime Mode. *Anal. Chem.* **2022**, *94*, 5190–5195. [CrossRef]
47. Wu, Q.; Wang, L.; Yan, Y.; Li, S.; Yu, S.; Wang, J.; Huang, L. Chitosan-Derived Carbon Dots with Room-Temperature Phosphorescence and Energy Storage Enhancement Properties. *ACS Sustain. Chem. Eng.* **2022**, *10*, 3027–3036. [CrossRef]
48. Ai, L.; Yang, Y.; Wang, B.; Chang, J.; Tang, Z.; Yang, B.; Lu, S. Insights into photoluminescence mechanisms of carbon dots: Advances and perspectives. *Sci. Bull.* **2021**, *66*, 839–856. [CrossRef]
49. Fen, M.; Wei, X.; Bin, L.; Zhen, Z.; Yan, F.; Hui, C.; Qing, H.; Jiang, C. Folding-Induced Spin–Orbit Coupling Enhancement for Efficient Pure Organic Room-Temperature Phosphorescence. *J. Phys. Chem. Lett.* **2022**, *13*, 1563–1570. [CrossRef]
50. Yi, C.; Yu, X.; Zhen, L. Room-Temperature Phosphorescence of Nicotinic Acid and Isonicotinic Acid: Efficient Intermolecular Hydrogen-Bond Interaction in Molecular Array. *J. Phys. Chem. Lett.* **2022**, *13*, 1652–1659. [CrossRef]

51. Nair, A.N.; Chava, V.S.N.; Bose, S.; Zheng, T.; Pilla, S.; Sreenivasan, S.T. In Situ Doping-Enabled Metal and Nonmetal Codoping in Graphene Quantum Dots: Synthesis and Application for Contaminant Sensing. *ACS Sustain. Chem. Eng.* **2020**, *8*, 16565–16576. [CrossRef]
52. Sheldon, R.A. Metrics of Green Chemistry and Sustainability: Past, Present, and Future. *ACS Sustain. Chem. Eng.* **2018**, *6*, 32–48. [CrossRef]
53. Zhang, T.; Gao, H.; Lv, A.; Wang, Z.; Gong, Y.; Ding, D.; Ma, H.; Zhang, Y.; Yuan, W.Z. Hydrogen bonding boosted the persistent room temperature phosphorescence of pure organic compounds for multiple applications. *J. Mater. Chem. C* **2019**, *7*, 9095–9101. [CrossRef]
54. Wang, X.; Wang, Z.; Feng, H.; Lin, C.; Shi, H.; An, Z.; Su, Z.-M.; Liang, F.-S. Activating room-temperature phosphorescence of 1,8-naphthalimide by doping into aromatic dicarboxylic acids. *Chem. Commun.* **2022**, *58*, 3641–3644. [CrossRef]